Erzincan Üniversitesi
Fen Bilimleri Enstitüsü Dergisi
2025, 18(1), 24-41
ISSN: 1307-9085, e-ISSN: 2149-4584
Araştırma Makalesi

Erzincan University
Journal of Science and Technology
2025, 18(1), 24-41
DOI: 10.18185/erzifbed.1397840
Research Article

High Efficiency and Wideband Polarization Converter Design in Terahertz Region

Fatih Kadiroğlu, Gökhan Öztürk

Atatürk Üniversitesi, Mühendislik Fakültesi, Elektrik Elektronik Mühendisliği, Erzurum, Türkiye 25100

Received: 29/11/2023, **Revised:** 17/01/2025, **Accepted:** 19/02/2025, **Published:** 28/03/2025

Abstract

In this study, the design of an adaptable, high-efficiency, and broadband polarization converter in the terahetz (THz) region was carried out in a computer environment with the electromagnetic simulation program CST Microwave Studio. Current density at the resonance frequencies of the designed model, reflection coefficients for the polarization converter, polarization conversion ratios, orthogonal components, and phase differences were examined in Excel graphics. The metamaterial designed as substrate Gold (Au), middle layer Rogers RT5880LZ, and top layer vanadium dioxide (VO_2)-Au composition, with the Bruggeman effect model, and the dielectric constant of VO_2 being taken as ε=9, has a Polarization Conversion Ratio (PCR), of over 90% in the range of 5.29-13.68 THz the relative bandwidth (RBW) was calculated as 88.40%. When the dielectric constant of VO_2 is taken as ε=12 with the Drude model, the RBW is calculated as 89.39% with a PCR of over 90% in the range of 5.20-13.61 THz. The designed model is 5.4 µm thick, adaptable, and highly efficient. In addition, a dynamic metamaterial was designed because the conductivity level of VO_2 changes according to temperature. The proposed VO2-based THz metamaterial polarization converter offers a higher bandwidth and RBW compared to the converters found in the literature. In this regard, it is efficient for applications that require high bandwidth, such as telecommunications, imaging, sensor detection, and data storage.

Keywords: polarization converter, vanadium dioxide, metamaterial.

Terahertz Bölgesinde Yüksek Verimli ve Geniş Bant Polarizasyon Dönüştürücü Tasarımı

Öz

Bu çalışmada, terahetz (THz) bölgesinde uyarlanabilir, yüksek verimli ve geniş bant polarizasyon dönüştürücü tasarımı elektromanyetik benzetim programı olan CST Microwave Studio ile bilgisayar ortamında gerçekleştirilmiştir. Tasarlanan modelin rezonans frekanslarında akım yoğunluğu, polarizasyon dönüştürücü için yansıma katsayıları, polarizasyon dönüştürme oranları, ortogonal bileşenler ve faz farkları Excel ile grafikler incelenmiştir. Alttaş Altın (Au), orta katman Rogers RT5880LZ ve üst katman vanadyum dioksit (VO_2)-Au bileşimi şeklinde tasarlanan metamalzeme, Bruggeman etkili modeli ile VO_2'nin dielektrik sabiti ε=9 alındığında, 5,29-13,68 THz aralığında %90 üzeri polarizasyon dönüştürme oranına (PCR) sahip, göreceli bant genişliği (RBW) %88,40 olarak hesaplanmıştır. Drude modeli ile VO_2'nin dielektrik sabiti ε=12 alındığında ise, 5,20-13,61 THz aralığında %90 üzeri PCR'a sahip, RBW %89,39 olarak hesaplanmıştır. Tasarlanan model 5,4 µm kalınlığında, uyarlanabilir ve yüksek verimlidir. VO_2'nin sıcaklığa göre iletkenlik seviyesinin değişmesinden dolayı da dinamik bir metamalzeme tasarlanmıştır**.** Önerilen VO2 bazlı THz metamaterial polarizasyon dönücü literatürde yer alan dönüştürücülere nispeten yüksek bant genişliği ve RBW sunar. Bu yönüyle yüksek bant genişliği gerektiren telekominikasyon, görüntüleme, sensor algılama, veri depolama gibi uygulamalar için verimlidir.

Anahtar Kelimeler: THz, polarizasyon dönüştürücü, vanadyum dioksit, metamalzeme.

Corresponding Author: gokhan.ozturk@atauni.edu.tr
Fatih KADİROĞLU, https://orcid.org/ 0000-0001-5077-8601
Gökhan ÖZTÜRK, https://orcid.org/ 0000-0001-8106-0053

1. Introduction

In recent years, polarization converter designs, which are referred to as a fundamental feature of electromagnetic (EM) wave, have gained prominence in various applications such as information processing, imaging, and sensing [1]. Nowadays, polarization converters, when applied solely in a virtual environment, require a large amount of natural material to accumulate sufficient phase [2]. However, Metamaterials (MM) have the potential to address the shortcomings caused by polarization converter devices. As a two-dimensional structural form of MM, metasurfaces are being further explored due to their ease of fabrication, and integration with other devices. The frequency spectra of devices designed with metasurfaces have remained fixed and unalterable after fabrication. Nonetheless, this limitation has practical implications [3].

There are a limited number of studies in the literature related to Metasurface-based Terahertz (THz) polarization converters [1, 4-6]. THz waves are electromagnetic waves that generally fall within the electromagnetic spectrum ranging from 0.1 to 10 THz, with undefined limits. Despite occupying a broad range in the electromagnetic spectrum, THz waves remain relatively unexplored, offering opportunities for innovations, and new research areas [7]. THz waves have numerous applications. They not only contribute to wireless communication but also open doors to new technologies in imaging, defense industry, the Internet of Things (IOT), and communication in nano-scale wireless sensor networks [8-9].

Vanadium dioxide (VO_2), as a high-quality photoelectric functional material, is a unique insulator, and metal oxide. It undergoes a transition from an insulating phase to a conducting phase when subjected to external factors such as heat, light, or stress. By virtue of phase transition of VO_2 from insulating to metallic state, induced in subpicosecond time scale by moderate optical pump, ultrafast control of THz transmission is enabled. This is compared to bare VO_2 films where no switching dynamics are observed under similar conditions [10-11]. From the perspective of the phase transition temperature, VO_2 typically exhibits a transition temperature closer to room temperature, around 68 °C, making it more suitable for application conditions in technology. This transition temperature, along with the sharp changes in electrical and optical properties that occur during the phase transition, offers more possibilities for various applications [12].

THz polarization converters can also be utilized to achieve VO_2 thermal modulation. Lv et al. [13] theoretically investigated a new metamaterial using the phase transition material VO_2 for thermal-controlled metamaterials. Concerning thermal-controlled materials, VO_2 films have the ability to transition from insulator to metal through phase changes. Through this phase transition, the conductivity of VO_2 varies depending on different temperatures. In other words, VO_2-based metamaterials offer a significant advantage of strong adjustability in the THz band [14- 15]. Therefore, there is a need for research on the utilization of the adjustable properties of VO_2 for polarization converters.

In the literature, when looking at VO2-based THz metamaterial polarization converters [1,3,14,31-40], these studies provide wideband PCR, but their RBW performances are below 85%. Additionally, the bandwidths of some studies pose limitations for applications requiring wideband performance. Furthermore, in some studies in the literature, the dielectric constant of VO2 has been simulated using either the Bruggeman effective medium model or the Drude model [1,3,14,31-40]. To overcome all these disadvantages, this study proposes a VO2-based THz metamaterial polarization converter with both high RBW (88.40%) and efficiency for wideband applications (offering bandwidths of 8.38 GHz and 8.41 GHz).

2. Material and Methods

Polarization, being a fundamental property of electromagnetic (EM) waves representing the oscillation pattern of the electric field in space, has been a subject of research interest for scientists aiming to control and manipulate the polarization of EM waves in devices and techniques due to its essential role in various applications and devices sensitive to polarization, such as polarization beam splitters, wave plates and antennas [16-18]. The polarization of EM waves can be manipulated using traditional techniques such as the Faraday effect and the optical activity of crystals [18-21]. Birefringent crystals manipulate the polarization of EM waves by delaying the phase of one linear component compared to the orthogonal component [17, 19-20]. If the phase of one component, measured at the crystal's output, is delayed by multiples of 90 degrees compared to the other orthogonal component, a linearly polarized wave is transformed into a circular or elliptical polarized wave [22]. On the other hand, if the magnitudes of two orthogonal components are the same, and the phase difference is 90 degrees, the wave becomes circularly polarized. If the magnitudes of the two orthogonal components are not the same and the phase difference is 90 or equal in magnitude, but not 90 or 180 degrees, the wave becomes elliptically polarized. Similarly, if the birefringent crystal phase delay is 180 degrees, a linearly polarized wave transforms into an orthogonal linearly polarized wave. To have a specific phase delay, the crystal must have a specific thickness ($d = \Delta\Phi\lambda/2\pi$), where d is the thickness of the crystal, $\Delta\Phi$ is the phase difference, and λ is the wavelength. This implies that very thick or bulky crystals are required to manipulate polarization at large wavelengths. For example, to transform a horizontally polarized wave into a vertically polarized wave, the crystal thickness should be $\lambda/2$ [23]. In addition to their bulkiness, traditional techniques have a very narrow bandwidth and only allow polarization transformation at specific wavelengths [24]. Furthermore, polarization manipulation through traditional techniques is dependent on the angle of incidence of the incoming wave [25-26]. In other words, when using traditional techniques, as the angle of incidence increases, there is a decrease in the efficiency of polarization conversion [27]. Therefore, the limitations of large volume, narrow bandwidth, and angle dependence make traditional techniques incompatible with modern miniature polarization control devices [18, 21, 27-30]. To overcome these limitations, scientists have developed artificial structures called metamaterials and metasurfaces, which manipulate the polarization of EM waves.

In this study, the dielectric permittivity of VO_2 was taken as 9 using the Bruggeman effective model and simultaneously, it was taken as 12 using the Drude model and a comparison was made.

The Bruggeman Effective Model is a theoretical model used to calculate the dielectric properties of complex material mixtures. This model is particularly used to estimate the dielectric constants of heterogeneous material mixtures. The Bruggeman Effective Model can be employed to describe the dielectric behavior of a variety of material mixtures, but it is most commonly used to predict the dielectric constants of composite materials. The Bruggeman Effective Model is based on a complex mathematical equation and can vary depending on the ratios and properties of different phases. This model is an important tool for understanding the electromagnetic behavior of materials and for material design and simulations. Equation (3) is used to calculate the effective dielectric constant of a material mixture [1].

$$\omega_p = 2\pi \times 2175THz \tag{1}$$

$$\omega c = 2\pi \times 4.35THz \tag{2}$$

$$\varepsilon(VO_2) = \frac{1}{4}\left\{\varepsilon_d(2-3V) + \varepsilon_m(3V-1) + \sqrt{[\varepsilon_d(2-3V) + \varepsilon_m(3V-1)^2 + 8\varepsilon_d\varepsilon_m]}\right\} \tag{3}$$

Here, ε_d and ε_m characterize the dielectric constants of the insulating and metallic phases, respectively and V represents the volume fraction of the metallic component. Therefore, the dielectric constant of VO_2 can be obtained as desired through Equation (3) [1]. In Fu et al.'s (2022) [1] simulation, the relative permittivity of VO_2 was taken as 9, with a conductivity of approximately 200 S/m at 25°C. In this study, the dielectric constant $\varepsilon(VO_2)$ was also taken as 9 and the conductivity value was set at 200 S/m and a comparison was made by taking $\varepsilon(VO_2)$ as 12 with the Drude model.

If we need to explain the frequency-dependent dielectric constant of VO_2 using the Drude model,

$$\varepsilon(\omega) = \varepsilon_{(\infty)} - \frac{\omega_p^2(\sigma)}{(\omega^2 + i\gamma\omega)} \tag{4}$$

$$\varepsilon_{(\infty)} = 12 \tag{5}$$

$$\gamma = 5{,}75 \times 10^{13}\ rad/s \tag{6}$$

$$\omega_p^2(\sigma) = \frac{(\sigma)}{(\sigma_0)}\omega_p^2(\sigma_0) \tag{7}$$

$$\sigma_0 = 3 \times 10^5\ S/m \tag{8}$$

$$\omega_p(\sigma_0) = 1{,}40 \times 10^{15}\ rad/s \tag{9}$$

In general, the permeability of VO_2 in the THz region can be defined with the Drude model using Equation (4). In Equation (4), ω represents the angular frequency, Equation (5) denotes the high-frequency dielectric constant, Equation (6) represents the collision frequency, σ is the conductivity of VO_2 and $\omega_p(\sigma_0)$ denotes the plasma frequency. The relationship between VO_2's conductivity and plasma frequency can be expressed in Equation (7). In Equation (8), σ_0 is given in Equation (9) and ω_p (σ_0) is given in Equation (12). The phase transition of VO_2 will lead to a significant change in its electrical conductivity. The simulation process assumes that VO_2 is in the metallic phase (insulating phase) and its conductivity is 3×10^5 S/[31].

In the simulation process, the proposed device was designed using the CST Microwave Simulator. The simulation was carried out in the frequency domain using the FEM (Finite Element Method) numerical method. For the simulation, unit cell (infinite boundary conditions) boundary conditions were selected in the frequency domain. Rogers substrate was chosen due to its mechanical strength and low dielectric constant in the simulation. Additionally, VO2 material was selected for the metasurface to enable temperature-tunable polarization conversion.

The conductivity of VO_2 at different heating temperatures is partly shown in Table 1. The tunning of VO_2 conductivity can be implemented by temperature, external electric field, and pump light irradiate. The electrical and optical excitation can quickly and accurately trigger the phase transition of VO_2. For thermal modulation, it can be achieved by commercial heater board that can adjust the temperature range from 25 °C to 120 °C. Obviously, thermal modulation is relatively easy to implement [32].

Table 1. Conductivity of VO_2 at Different Temperatures [32]

Temperature/°C	35	60	67	69	80
Conductivity/(*S/m*)	200	820	21700	158000	212000

3. Results and Discussion

In this study, a metamaterial structure for a polarization converter operating in the THz region has been designed, considering the dielectric constant of VO_2 using the Bruggeman effective model with ε=9 and the Drude model with ε=12. This model consists of a top layer composed of VO_2-Au composite, a middle layer of Rogers RT5880LZ and an Au substrate used as the bottom layer. It is designed as a single-layer, high-efficiency, adaptable and wideband polarization converter in the THz region (Figure 1). Additionally, the study investigates the effects of structural parameters, polarization angles and incident angles on the polarization conversion performance.

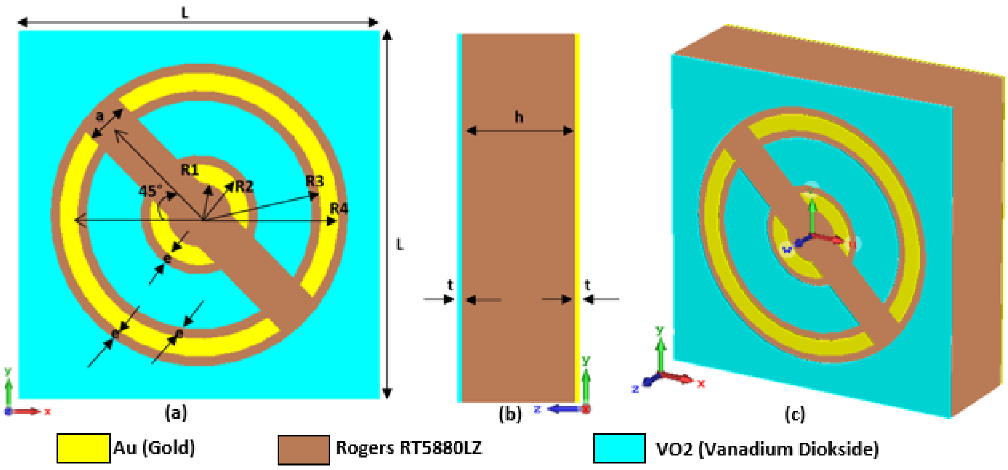

Figure 1. The created polarization converter: (a) Front view, (b) Side view, (c) Perspective view and material structure.

Figure 1 shows the front, side and perspective view of the designed polarization converter. Table 2 lists the dimensions of the functioning model. The aspect ratio of the created metamaterial is L-L 16-16 and its thickness h+2t is 5.4 µm.

Table 2. Dimensions of the created polarization converter

Measurement Parameter	R1	R2	R3	R4	h	t	L	a	e
Value (µm)	1.4	2.2	5.4	6.2	5	0.2	16	2	0.4

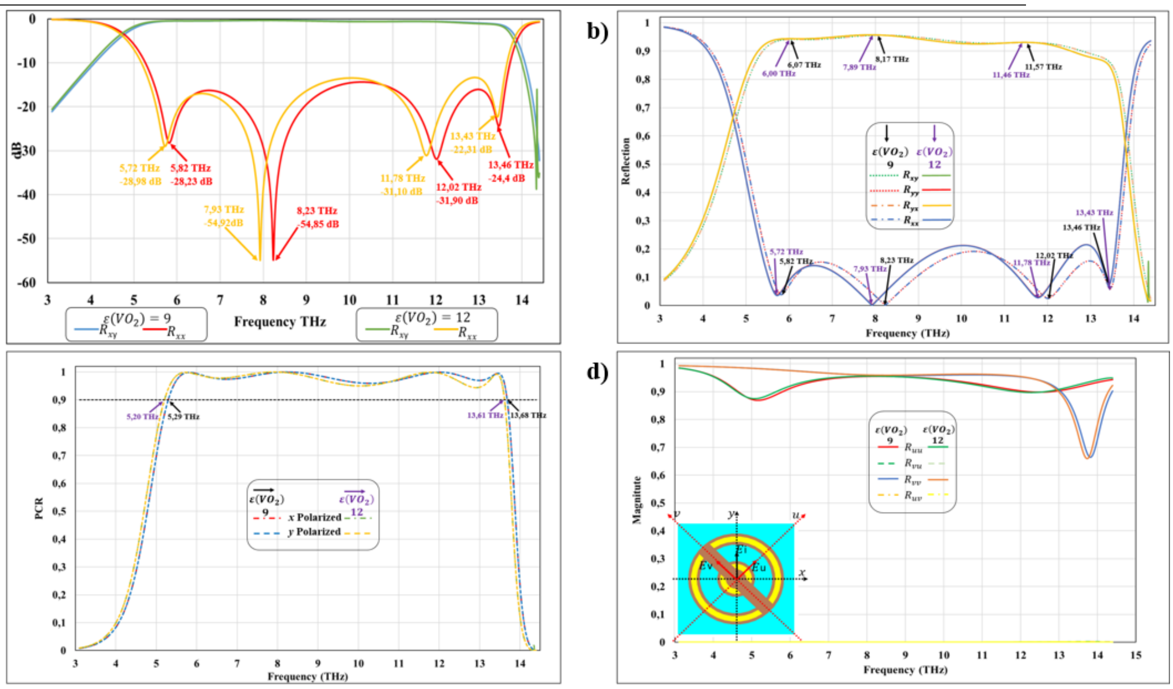

Figure 2. a) R_{xx} and R_{xy} graphs, b) reflection graph, c) PCR, d) graph of the orthogonal components of the designed metamaterial

When examining the dB graph provided in Figure 2 (a) for the designed metamaterial, using the Bruggeman effective model with a dielectric constant (ε) of 9 for VO_2, four resonance points are observed at 5.82 THz with a value of -28.23 dB, 8.23 THz with a value of -54.85 dB, 12.02

THz with a value of -31.90 dB and 13.46 THz with a value of -24.4 dB. When the dielectric constant (ε) for VO_2 is taken as 12 using the Drude model, four resonance points are observed at 5.72 THz with a value of -28.98 dB, 7.93 THz with a value of -54.92 dB, 11.78 THz with a value of -31.10 dB and 13.43 THz with a value of -22.31 dB.

Table 3. Comparison of resonance points for the created polarization converter with VO_2 dielectric constant ε=9 and ε=12

VO_2 Epsilon		**Rezonans 1**	**Rezonans 2**	**Rezonans 3**	**Rezonans 4**
ε=9	**Frekans (THz)**	5.82	8.23	12.02	13.46
	Genlik (dB)	-28.23	-54.85	-31.90	-24.4
ε=12	**Frekans (THz)**	5.72	7.93	11.78	13.43
	Genlik (dB	-28.98	-54.92	-31.10	-22.31

In Figure 2 (b), graphs corresponding to the calculated reflection coefficients based on the data from the R_{xx} and R_{xy} graphs in Figure 2 (a) are provided. As shown in Figure 2 (b), when examining the magnitude graph of the cross-polarized reflection coefficients $|R_{xy}|$ and $|R_{yx}|$, it can be observed that for the VO_2 dielectric constant taken as ε=9 using the Bruggeman effective model, the cross-polarity coefficients $| R_{xy} |$ and $| R_{yx} |$ are greater than 0.9 in the range of 5.29-13.68 THz and for the VO_2 dielectric constant taken as ε=12 using the Drude model, the cross-polarity coefficients $|R_{xy}|$ and $|R_{yx}|$ are also greater than 0.9 in the range of 5.20-13.61 THz. Furthermore, it is worth noting that the cross-polarization reflection curves have three peak values at 6.07, 8.17 and 11.57 THz when the VO_2 dielectric constant is taken as ε=9 using the Bruggeman effective model and three peak values at 6.00, 7.89 and 11.46 THz when the VO_2 dielectric constant is taken as ε=12 using the Drude model. Additionally, the co-reflection coefficients $|R_{yy}|$ and $|R_{xx}|$ are almost zero at the resonance peak points. In other words, almost all *y* or *x*-polarized waves can transform cross-polarization, i.e., *x* or *y* polarization, respectively, at the resonance peaks.

Table 4. Interpretation of the reflection graphs of the created polarization converter according to the VO_2 dielectric constant

	Bruggeman Effective Model	**Drude Model**
VO_2 Dielectric Constant	ε=9	ε=12
THz >0.9 (dB)	5.29-13.68	5.20-13.61
Peak 1 (THz)	6.07	6.00
Peak 2 (THz)	8.17	7.89
Peak 3 (THz)	11.57	11.46

To better explain the conversion efficiency, the PCR for the *y*-polarized wave

$$PCR = \frac{|r_{xy}|^2}{\left(|r_{xy}|^2+|r_{y,y}|^2\right)} \tag{10}$$

Based on Equation (10), on the other hand, as the electric field of incident wave keeps along *x* direction, the alphabets of *x* and *y* are interchanged with each other. In Figure 2 (c), when ε(VO_2)

is 9 using the Bruggeman effective model, it can be observed that the polarization conversion ratio (PCR) for the normal angle (5.29-13.68 THz) has efficiency of over 90%. The PCR value reaches approximately 1 at the resonant frequencies of 5.82 THz, 8.23 THz, 12.02 THz and 13.46 THz. When ε(VO_2) is 12 using the Drude model, it is observed that the polarization conversion ratio (PCR) for the normal angle (5.20-13.61 THz) has efficiency of over 90%. The PCR value reaches approximately 1 at the resonant frequencies of 5.72 THz, 7.93 THz, 11.78 THz and 13.43 THz. It is concluded that at the resonant frequencies, an almost purely *x* (*y*) polarized event can be transformed into *y* (*x*) components.

Table 5. Interpretation of the reflection graph of the generated polarization converter based on the VO_2 dielectric constant and PCR

VO_2 Dielectric Constant	**Frequency Range (THz)**	**PCR**
ε=9	5.29-13.68	88.40%
ε=12	5.20-13.61	89.39%

To understand the working principle of the proposed polarization conversion device, the reflected and incident waves can be separated into orthogonal components, denoted by u and v directions in the model shown in Figure 2 (d). The u and v axes are rotated 45° with respect to the *z*-axis, relative to the *x* and *y* axes. As shown in Figure 2 (d), assuming that the incoming wave, which is *y*-polarized under normal incidence, can be decomposed into two orthogonal components (E_u and E_v) along the *u*-axis and *v*-axis, the incoming electric field can be expressed as follows [1].

$$E_i = E_i exp(jkz)\hat{e}_u + E_i exp(jkz)\hat{e}_v \tag{11}$$

The reflected electric field

$$E_r = \{R_{uu}E_i exp[j(-kz + \varphi_{uu})] + R_{uv}E_i exp[j(-kz + \varphi_{uv})]\}\hat{e}_u + \{R_{vv}E_i exp[j(-kz + \varphi_{vv})] + R_{vv}E_i exp[j(-kz + \varphi_{vu})]\}\hat{e}_v \tag{12}$$

Here, R_{uu}, R_{vu}, R_{vv} and R_{uv} represent the magnitudes of the reflection coefficients for *u-u*, *u-v*, *v-to-v*, and *v-u* polarization transformations, respectively. Additionally, φ_{uu}, φ_{vu}, φ_{vv}, and φ_{uv} are the corresponding phases. Linearly polarized waves can be obtained when $R_{uu} = r_{vv} = R$, $R_{vu} = R_{uv} = 0$, *and* $\Delta\varphi = \varphi_{uu} - \varphi_{vv} = 2n\pi \pm \pi$ $(n \in Z)$. In Figure 2 (d), it can be observed that the orthogonal components R_{uv} and R_{vu} are approximately close to zero, the R_{vv} component is greater than 0.9 throughout the entire band and R_{uu} is greater than 0.87 across the entire band. This means that the upper resonant structure has no polarization transformation effect on *u*. The *u*- and *v*-polarized components have equal magnitudes only for the same common polarization. The graph of orthogonal components shows that the designed metamaterial has good polarization conversion properties.

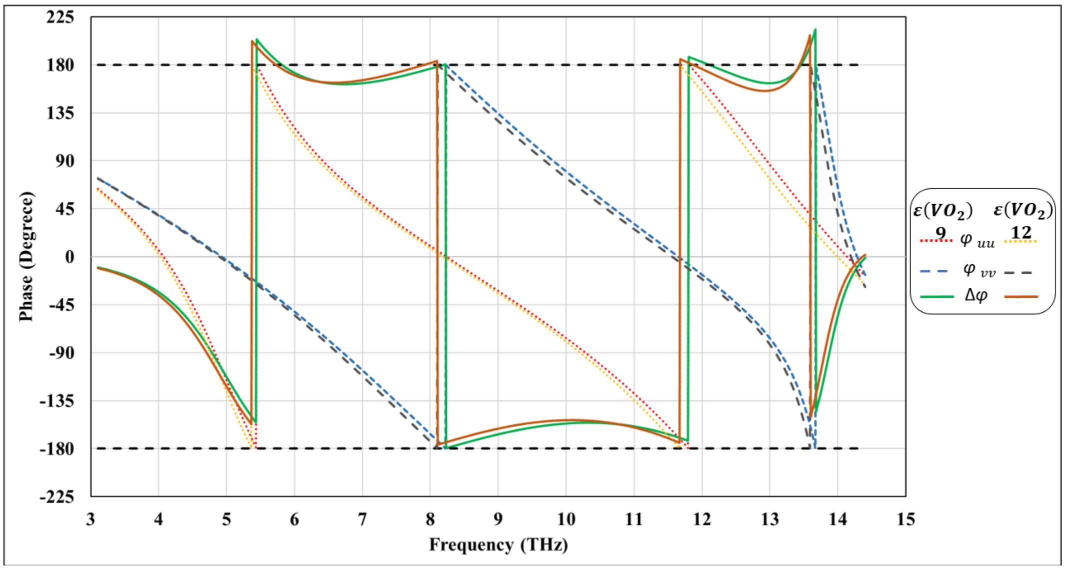

Figure 3. Phase difference plot of the designed metamaterial

Figure 3 shows that with the Bruggeman effective model and ε(VO_2) = 9, in the 5.29-13.68 THz working range, the phase differences of the orthogonal components are ±180° (±24°) at four resonance frequencies: 5.82 THz, 8.23 THz, 12.02 THz and 13.46 THz. When using the Drude Model and ε(VO_2) = 12, the phase differences in the 5.20-13.61 THz working range are ±180° (±26°) at four resonance frequencies: 5.72 THz, 7.93 THz, 11.78 THz and 13.43 THz. The phase difference plot demonstrates that the designed metamaterial has excellent polarization conversion capabilities.

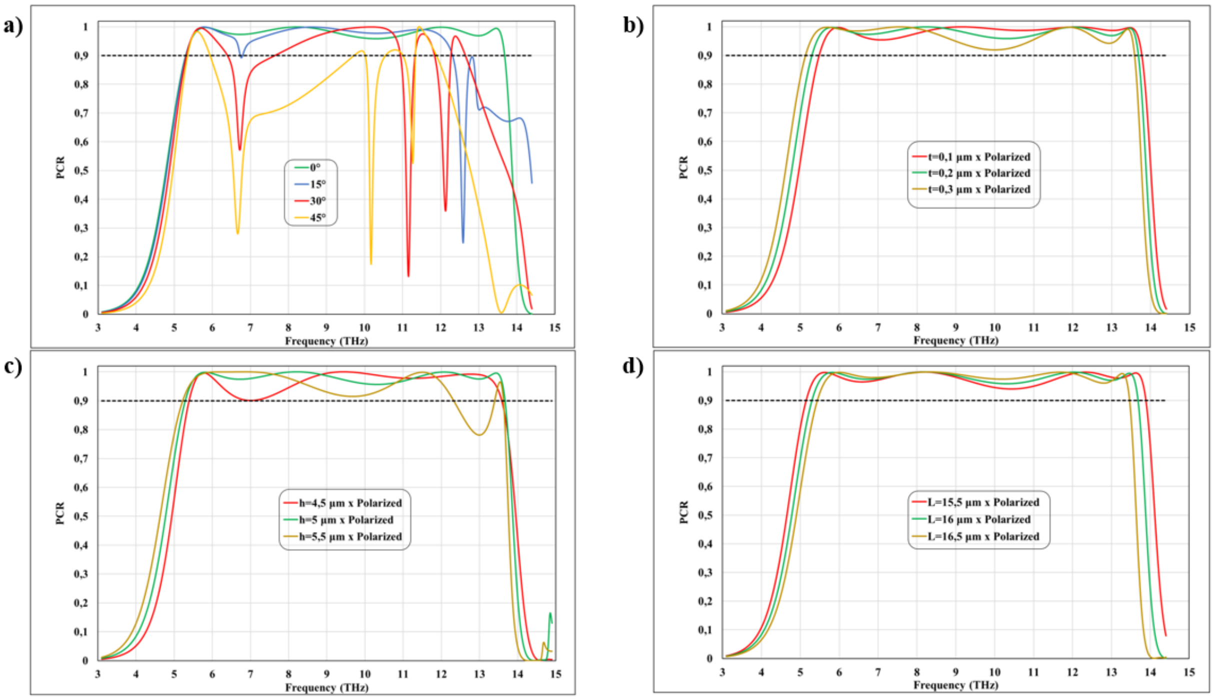

Figure 4. a) PCR graph according to the incident angle of the designed metamaterial, PCR plot of the designed model for different thickness parameters b) t, c) h, d) L

Figure 4 (a) shows that as the angle of incidence increases from 0° to 45°, the PCR bandwidth decreases and beyond 15°, the PCR graph deteriorates significantly. Therefore, it demonstrates that the designed metamaterial is sensitive to the angle of incidence. The designed model performs best at normal incidence.

When $\varepsilon(VO_2)=9$ is used with the Bruggeman effective model, a comparative graph of the thickness (t) of the VO_2-Au composite in the top layer and the Au surface in the top layer of the designed model with one lower and one upper thickness value is shown in Figure 4 (b). From this graph, it can be observed that when the thickness of the upper and lower layer materials is proportionally increased or decreased, as the thickness increases, the bandwidth shifts to a lower step, and the PCR graph begins to deteriorate. The VO_2-Au composite in the top layer and the Au surface in the top layer are not included in the graph for their next lower and upper step thicknesses ($t<0.1$ μm and $t>0.3$ μm) because the degradation is more significant. Accordingly, it can be seen that the most suitable PCR value in the designed model is at $t=0.2$ μm.

When $\varepsilon(VO_2)=9$ is used with the Bruggeman effective model, a comparative graph of the designed model's middle material thickness (h) with one lower and one upper thickness value is shown in Figure 4 (c). From this graph, it can be observed that when the thickness of the middle layer material is proportionally increased or decreased, as the thickness increases, the bandwidth shifts to a lower step, and the PCR graph begins to deteriorate. The VO_2-Au composite in the top layer and the Au surface in the top layer are not included in the graph for their next thicknesses ($h<4.5$ μm and $h>5.5$ μm) because the degradation is more significant. However, it can be seen that the most suitable PCR value in the designed model is at $h=5$ μm.

When $\varepsilon(VO_2)=9$ is used with the Bruggeman effective model, a comparative graph of the middle layer, which is the Rogers RT5880LZ of the designed model, is drawn in Figure 4 (d) in proportion to the lower and upper values of the width-length ratio (L). It can be observed from this graph that when the middle layer material's L is reduced from $L=16$ μm to $L=15.5$ μm, the bandwidth increases, but the PCR graph begins to deteriorate. Likewise, when the middle layer material's L is increased from $L=16$ μm to $L=16.5$ μm, the bandwidth narrows, but the PCR graph begins to improve. The VO_2-Au composite in the top layer and the Au surface in the top layer are not included in the graph for their next thicknesses ($L<15.5$ μm and $L>16.5$ μm) since the variation begins to increase. However, it can be observed that the most suitable PCR value in the designed model is at $L=16$ μm.

Similarly, when $\varepsilon(VO_2)=12$ is used with the Drude model, the effect of t (thickness), h (thickness) and L (width-length) parameter changes on the PCR graph can be seen from the graphs in Figure 2, similar changes can be observed in Figure 4.

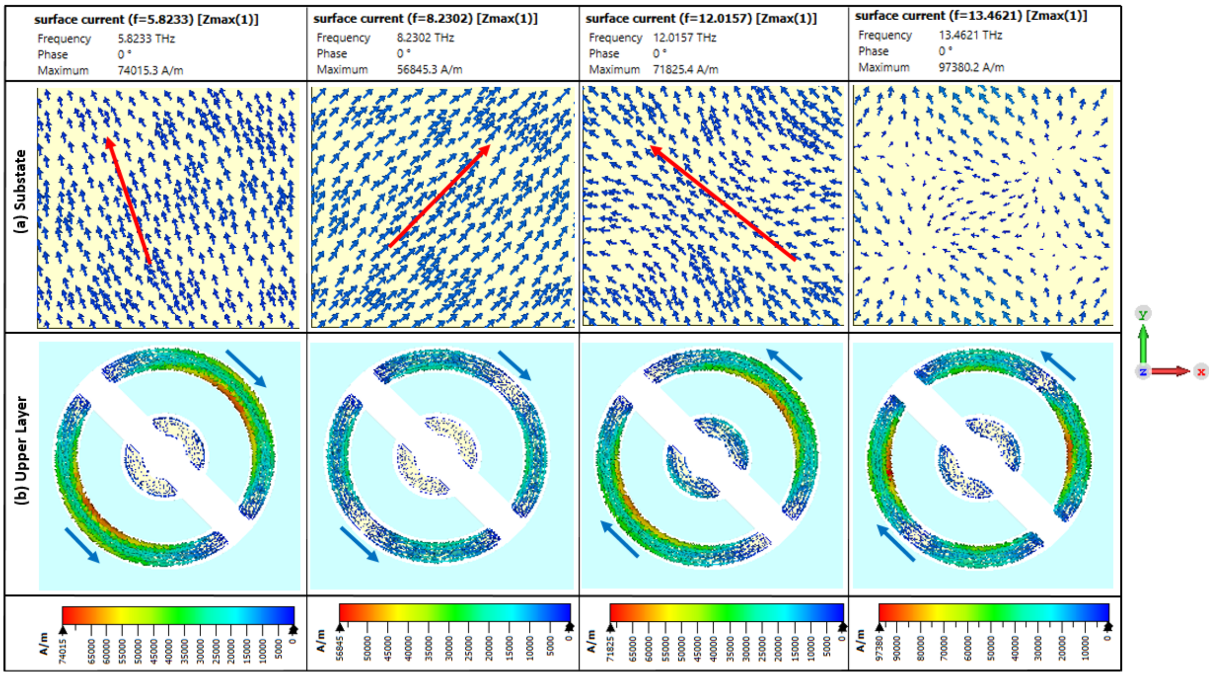

Figure 5. Current densities with ε(VO2)=9 in the designed model

In Figure 5, current densities at the resonance points of 5.82 THz, 8.23 THz, 12.02 THz and 13.46 THz were plotted using the CST program.

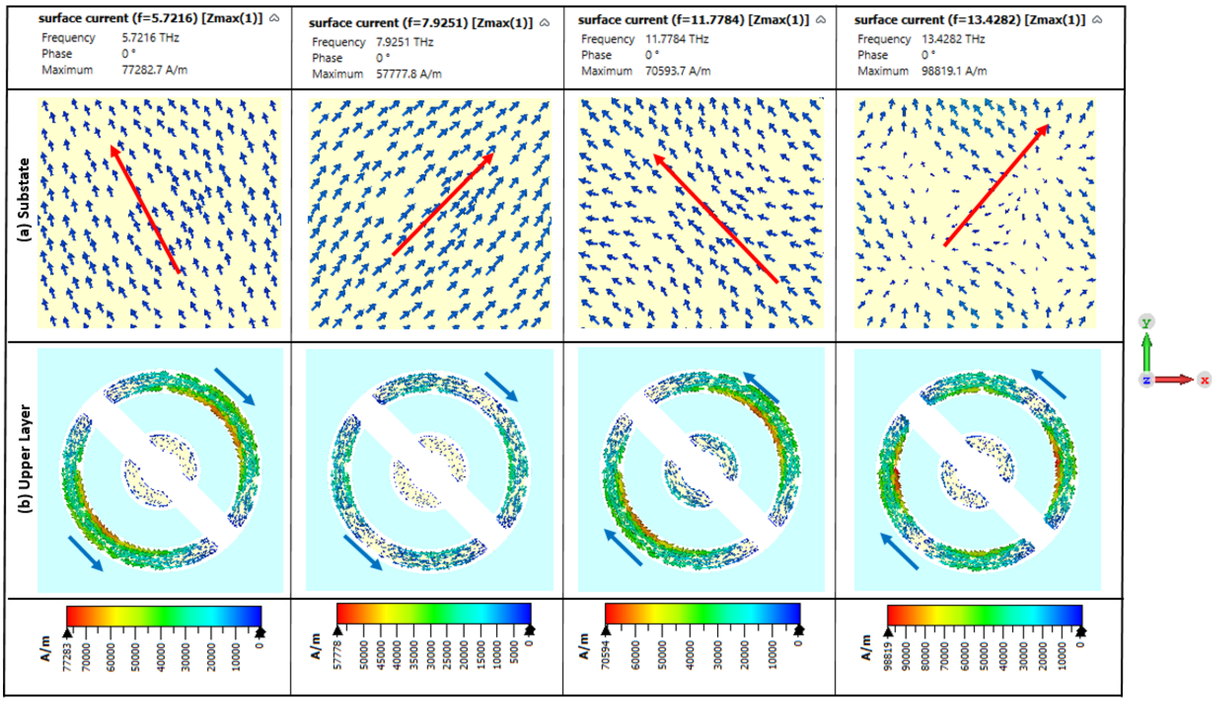

Figure 6. Current densities with ε(VO2)=12 in the designed model

In Figure 6, current densities at the resonance points of 5.72 THz, 7.93 THz, 11.78 THz and 13.43 THz were plotted using the CST program.

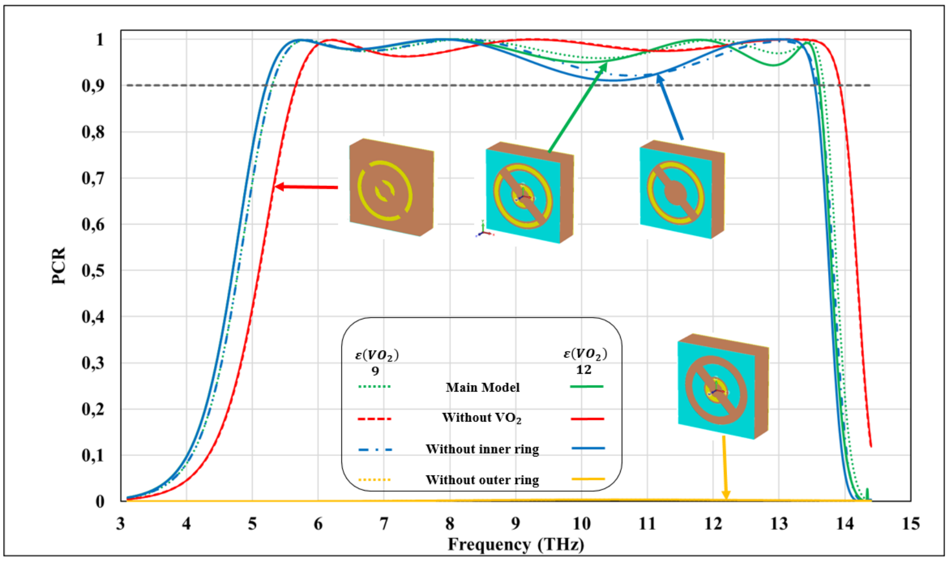

Figure 7. PCR graph of the effect of the parts of the designed metamaterial

In Figure 7, the PCR data of the designed metamaterial, the version with VO_2 removed, the version with inner ring removed and the version with the outer ring made of gold are plotted on the same graph. Using the data obtained from Figure 7 with $\varepsilon(VO_2)$ 9 for the Bruggeman effective model and $\varepsilon(VO_2)$ 12 for the Drude model, the effects of RBW and PCR for the structures used in the metamaterial were examined, as summarized in Table 7. According to the PCR results for the Drude and Bruggeman models shown in Figure 7, the average PCR variation obtained between the two models shows a change of 1.109%.

Table 7. Effects of components in the metamaterial on polarization conversion

Parameters	**Type of Model**				
	Main Model		**Without Inner Ring**		**Without VO_2**
$\boldsymbol{\varepsilon(VO_2)}$	9	12	9	12	-
PCR Frequency Range Above 90% (THz)	5.29-13.68	5.20-13.61	5.18-14.12	5.20-13.54	5.65-13.91
Bandwidth THz (RBW)	8.38	8.41	8.94	8.34	8.26
RBW	88.40%	89.39%	92.67%	88.99%	84.41%
PCR >96%	5.46-13.62 THz	5.35-9.62 THz & 10.47-12.64 THz	5.46-9.46 THz & 11.98-13.47 THz	5.36-9.09 THz & 11.70-13.48 THz	5.65-13.79 THz
>96% PCR Bandwidth (THz)	8.16	6.44	5.49	5.51	8.14

As can be seen in Table 7, which was created based on this graph, it was observed that by removing the inner ring, the RBW increased by 0.5 THz compared to the main model, but the conversion rate frequency range above 96% of the PCR band gap decreased. When VO_2 is removed, it is seen that both RBW and PCR bandwidth decrease, thus the effect of VO_2 on the metamaterial is observed.

a) b)

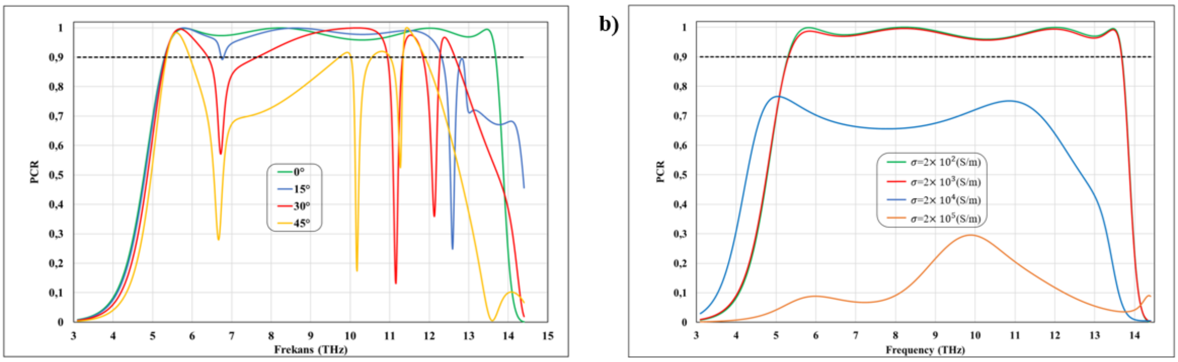

Figure 8. a) PCR with different incident angles under y-polarized wave at the temperature of 25°C, b) PCR graph for the designed model with different conductivity levels of VO_2.

Figure 8 (a) shows the PCR graph of the designed metamaterial as a function of the angle of incidence. It can be observed that the PCR bandwidth decreases as the wave angle increases from 0° to 45°, and the PCR graph deteriorates significantly after 15°. Therefore, it indicates that the designed metamaterial is sensitive to the angle of incidence, and it performs best at normal incidence angles.

As observed in the graph, as shown in Table 7, removing the inner ring increases the RBW by 0.5 THz compared to the main model. However, it is also seen that the PCR bandwidth with a conversion rate of over 96% decreases. When VO_2 is removed, both RBW and PCR bandwidth decrease, indicating the impact of VO_2 on the metamaterial.

Since VO_2 has varying conductivity levels depending on temperature, the PCR graph was plotted for VO_2 with conductivity values ranging from $\sigma = 200$ (S/m) at 25°C to $\sigma = 2\times10^5$ (S/m) (Figure 8 (b)). This way, the effect of VO_2's temperature-dependent conductivity on the designed metamaterial is observed. As the conductivity of VO_2 changes with temperature, it is seen that the VO_2 film transitions from an insulating state to a metallic state, which can lead to a phase transition of electromagnetic waves. Therefore, a dynamic polarization converter design was realized.

When reviewing the literature for polarization converters using VO_2 in the THz region, no comparisons were found regarding the use of Bruggeman effective model and Drude model with VO_2's dielectric constant. The results obtained in this thesis work are compared with some of the THz polarization converters found in the literature, as shown in Table 8. As observed in Table 8, the dielectric constant of VO_2 with the Bruggeman effective model offers polarization conversion with a bandwidth of 8.38 THz, and with the Drude model, it provides a bandwidth of 8.41 THz, and no similar study with a thickness of less than 5.4 μm has been found.

Table 8. Comparison of the proposed polarization vonverter with other studies in the literature

Reference	$\boldsymbol{\varepsilon(VO_2)}$	**Bant Aralığı (THz)**	**Bant Genişliği (THz)**	**PCR**	**RBW**	**Kalınlık (μm)**
Xiao *et al.* 2017 [33]	9	2.10-5.03	2.93	>90%	82.19%	10.4
Zheng *et al.* 2018 [14]	9	4.95-9.39	4.44	>90%	61.92%	4.42
Yang *et al.* 2018 [34]	9	2.06–4.26	2.2	>90%	69.62%	11.4
Zhang *et al.* 2020 [35]	12	1.38-1.85	0.47	>90%	29.10%	34.36
Yang *et al.* 2020 [36]	12	1.99-3.46	1.47	>90%	53.94%	34.4
Zhang *et al.* 2021 [37]	N	0.744-1.782	1.04	>90%	82.19%	30.3
Zhang *et al.* 2022 [38]	N	0.68–1.60	0.92	>90%	80.70%	47.6
Yu *et al.* 2022 [3]	9	2.22-5.42	3.2	>90%	83.77%	10.4
Yu *et al.* 2022 [1]	9	2.03-5	2.97	>89%	84.50%	10.4
Zhang *et al.* 2023 [32]	12	2.9–8.4	5.5	>90%	97.35%	18.9
Niu *et al.* 2023 [31]	12	2.54–4.55	2.01	>90%	56.70%	8.84
Lian *et al.* 2023 [39]	12	2.12–3.58	1.46	>90%	51.23%	30
Lian *et al.* 2023 [40]	12	0.49–1.87	1.38	>90%	116.95%	66
This Work	**9**	**5.29-13.68**	**8.38**	**>90%**	**88.40%**	**5.4**
	12	**5.20-13.61**	**8.41**	**>90%**	**89.39%**	

4. Conclusion

In this study, a single-layer, high-efficiency, and wideband polarization converter was designed in the THz region using a VO_2-Au composite upper layer, a Rogers RT5880LZ middle layer, and Au as the substrate material. Comparisons were made in the designed metamaterial using the Bruggeman effective model with ε(VO_2) 9 and the Drude model with ε(VO_2) 12. When the VO_2-based metamaterial was designed using the Bruggeman effective model with ε(VO_2) 9, the PCR frequency range of 90% and above was found to be 5.29-13.68 THz with a relative bandwidth (RBW) of 88.40%, and the PCR value was calculated to be at least 96% in the 5.46-13.62 THz range. Similarly, when the Drude model was used with ε(VO_2) 12, the PCR frequency range of 90% and above was found to be 5.20-13.61 THz with an RBW of 89.39%, and the PCR value was calculated to be at least 96% in the 5.35-9.62 THz and 10.47-12.64 THz ranges. The proposed VO2-based THz metamaterial polarization converter offers PCR performance for both the Bruggeman and Drude models compared to the studies in the literature. Additionally, it provides superior PCR performance for a wider bandwidth (8.41 GHz for the Drude model and 8.38 GHz for the Bruggeman model) and RBW (88.40% for the Drude model and 89.39% for the Bruggeman model) relative to similar studies. The outer ring located in the upper layer, apart from the middle and lower layers, was found to be an important factor in the created metamaterial, enhancing the polarization conversion effect. The inner ring was found to increase the polarization conversion effect, and the use of VO_2 increased the polarization conversion rate to some extent. A dynamic metamaterial was designed due to the change in the VO_2's conductivity level with temperature. Using a VO_2-Au composite upper layer, a Rogers RT5880LZ middle layer, and Au as the substrate material, an adaptable, highly efficient model was created with a bandwidth of approximately 8.38 THz when ε(VO_2) 9 was used and approximately 8.41 THz when ε(VO_2) 12 was used, enabling polarization conversion of 90% and above, with a thickness of 5.4 μm.

Ethics in Publishing

There are no ethical issues regarding the publication of this study.

References

[1] Yu, F. Y., Zhu, J. B., & Shen, X. B. (2022). Tunable and reflective polarization converter based on single-layer vanadium dioxide-integrated metasurface in terahertz region. Optical Materials, 123, 111745.

[2] Grosjean, T., Baida, F., Adam, R., Guillet, J. P., Billot, L., Nouvel, P., Torres, J., Penarier, A., Charraut, D., & Chusseau, L. (2008). Linear to radial polarization conversion in the THz domain using a passive system. Optics express, 16(23), 18895-18909.

[3] Yu, F. Y., Shang, X. J., Fang, W., Zhang, Q. Q., Wu, Y., Zhao, W., Liu, J., Song, Q., Wang, C., Zhu, J., & Shen, X. B. (2022). A terahertz tunable metamaterial reflective polarization converter based on vanadium oxide film. Plasmonics, 17(2), 823-829.

[4] Song, Z., Zhu, J., Zhu, C., Yu, Z., & Liu, Q. (2015). Broadband cross polarization converter with unity efficiency for terahertz waves based on anisotropic dielectric meta-reflectarrays. Materials Letters, 159, 269-272.

[5] Zhang, J., Tian, J., Xiao, S., & Li, L. (2020). Methodology for high purity broadband near-unity THz linear polarization converter and its switching characteristics. IEEE Access, 8, 46505-46517.

[6] Guo, Y., Xu, J., Lan, C., & Bi, K. (2021). Broadband and high-efficiency linear polarization converter based on reflective metasurface. Engineered Science, 14(2), 39-45.

[7] Akkaş, M. A. (2018). Terahertz Teknolojisi Uygulamaları ve Terahertz Dalgalarının Kablosuz Haberleşme için Elektromanyetik Modellemesi. Afyon Kocatepe Üniversitesi Fen ve Mühendislik Bilimleri Dergisi, 18(1), 190-200.

[8] Nagatsuma, T., Ducournau, G., & Renaud, C. C. (2016). Advances in terahertz communications accelerated by photonics. Nature Photonics, 10(6), 371-379.

[9] Pawar, A. Y., Sonawane, D. D., Erande, K. B., & Derle, D. V. (2013). Terahertz technology and its applications. Drug invention today, 5(2), 157-163.

[10] Fu, G., Polity, A., Volbers, N., & Meyer, B. K. (2006). Annealing effects on VO2 thin films deposited by reactive sputtering. Thin Solid Films, 515(4), 2519-2522.

[11] Choi, S. B., Kyoung, J. S., Kim, H. S., Park, H. R., Park, D. J., Kim, B. J., Ahn, Y. H., Rotermund, F., Kim, H.T., Ahn, K. J., & Kim, D. S. (2011). Nanopattern enabled terahertz all-optical switching on vanadium dioxide thin film. Applied Physics Letters, 98(7).

[12] Wu, C., Feng, F., & Xie, Y. (2013). Design of vanadium oxide structures with controllable electrical properties for energy applications. Chemical Society Reviews, 42(12), 5157-5183.

[13] Lv, T. T., Li, Y. X., Ma, H. F., Zhu, Z., Li, Z. P., Guan, C. Y., Shi, J. H., Zhang, H., & Cui, T. J. (2016). Hybrid metamaterial switching for manipulating chirality based on VO2 phase transition. Scientific reports, 6(1), 23186

[14] Zheng, X., Xiao, Z., & Ling, X. (2018). A tunable hybrid metamaterial reflective polarization converter based on vanadium oxide film. Plasmonics, 13, 287-291.

[15] Qiu, Y., Yan, D. X., Feng, Q. Y., Li, X. J., Zhang, L., Qiu, G. H., & Li, J. N. (2022). Vanadium dioxide-assisted switchable multifunctional metamaterial structure. Optics Express, 30(15), 26544-26556.

[16] Lin, B., Lv, L., Guo, J., Liu, Z., Ji, X., & Wu, J. (2020). An ultra-wideband reflective linear-to-circular polarization converter based on anisotropic metasurface. IEEE Access, 8, 82732-82740.

[17] Kamal, B., Chen, J., Yingzeng, Y., Ren, J., Ullah, S., & Khan, W. U. R. (2021). High efficiency and ultra-wideband polarization converter based on an L-shaped metasurface. Optical Materials Express, 11(5), 1343-1352.

[18] Li, Z. Y., Li, S. J., Han, B. W., Huang, G. S., Guo, Z. X., & Cao, X. Y. (2021). Quad-band transmissive metasurface with linear to dual-circular polarization conversion simultaneously. Advanced theory and simulations, 4(8), 2100117.

[19] Mei, Z. L., Ma, X. M., Lu, C., & Zhao, Y. D. (2017). High-efficiency and wide-bandwidth linear polarization converter based on double U-shaped metasurface. Aip Advances, 7(12).

[20] Lin, B. Q., Lv, L. T., Guo, J. X., Wang, Z. L., Huang, S. Q., & Wang, Y. W. (2020). Ultra-wideband linear-to-circular polarization conversion metasurface. Chinese Physics B, 29(10), 104205.

[21] Nguyen, T. K. T., Nguyen, T. M., Nguyen, H. Q., Cao, T. N., Le, D. T., Bui, X. K., Bui, S. T., Truong, C. L., Vu, D. L., & Nguyen, T. Q. H. (2021). Simple design of efficient broadband multifunctional polarization converter for X-band applications. Scientific Reports, 11(1), 2032.

[22] Xu, G., Gao, L., Chen, Y., Ding, Y., Wang, J., Fang, Y., Wu, X., & Sun, Y. (2022). Broadband polarization manipulation based on W-shaped metasurface. Frontiers in Materials, 9, 850020.

[23] Khan, M. I. (2018). Design and Analysis of Metasurfaces for Polarization Conversion of Electromagnetic Waves (Doctoral dissertation, National University of Science & Technology, Islamabad).

[24] Zhao, J., & Cheng, Y. (2016). A high-efficiency and broadband reflective 90 linear polarization rotator based on anisotropic metamaterial. Applied Physics B, 122, 1-7.

[25] Khan, M. I., Hu, B., Amanat, A., Ullah, N., Khan, M. J. I., & Khalid, A. R. (2020). Efficient asymmetric transmission for wide incidence angles using bi-layered chiral metasurface. Journal of Physics D: Applied Physics, 53(30), 305004.

[26] Couto, M. M., Silva, M. W. B., & Campos, A. L. P. S. (2021). A novel ultra-wideband reflective cross-polarization converter based on anisotropic metasurface. Journal of Electromagnetic Waves and Applications, 35(12), 1652-1662.

[27] Xu, J., Li, R., Wang, S., & Han, T. (2018). Ultra-broadband linear polarization converter based on anisotropic metasurface. Optics Express, 26(20), 26235-26241.

[28] Gao, J., Wang, C., Qiang, T., Zhang, K., & Wu, Q. (2018). Multifunctional polarization converter based on dielectric metamaterial. physica status solidi (a), 215(11), 1700535.

[29] Khan, M. I., Khalid, Z., & Tahir, F. A. (2019). Linear and circular-polarization conversion in X-band using anisotropic metasurface. Scientific reports, 9(1), 4552.

[30] Lin, B. Q., Lv, L. T., Guo, J. X., Wang, Z. L., Huang, S. Q., & Wang, Y. W. (2020). Ultra-wideband linear-to-circular polarization conversion metasurface. Chinese Physics B, 29(10), 104205.

[31] Niu, J., Yao, Q., Mo, W., Li, C., & Zhu, A. (2023). Switchable bi-functional metamaterial based on vanadium dioxide for broadband absorption and broadband polarization in terahertz band. Optics Communications, 527, 128953.

[32] Zhang, G., Wu, Q., Zhong, Z., & Zhang, B. (2023). Bifunctional metasurface for cross-polarization conversion and ultra-broadband absorption in terahertz range. Optics Communications, 531, 129181.

[33] Xiao, Z., Zou, H., Zheng, X., Ling, X., & Wang, L. (2017). A tunable reflective polarization converter based on hybrid metamaterial. Optical and Quantum Electronics, 49, 1-11.

[34] Yang, X., Zhang, B., & Shen, J. (2018). An ultra-broadband and highly-efficient tunable terahertz polarization converter based on composite metamaterial. Optical and Quantum Electronics, 50, 1-11.

[35] Zhang, J., Zhang, K., Cao, A., Liu, Y., & Kong, W. (2020). Bi-functional switchable broadband terahertz polarization converter based on a hybrid graphene-metal metasurface. Optics Express, 28(18), 26102-26110.

[36] Yang, C., Gao, Q., Dai, L., Zhang, Y., Zhang, H., & Zhang, Y. (2020). Bifunctional tunable terahertz circular polarization converter based on Dirac semimetals and vanadium dioxide. Optical Materials Express, 10(9), 2289-2303.

[37] Zhang, X., Ye, H., Zhao, Y., & Zhang, H. (2021). A tunable ultra-wideband cross-polarization conversion based on the band splicing technology. Applied Physics B, 127, 1-11.

[38] Zhang, H., He, X., Zhang, D., & Zhang, H. (2022). Multitasking device with switchable and tailored functions of ultra-broadband absorption and polarization conversion. Optics Express, 30(13), 23341-23358.

[39] Lian, X., Ma, M., Tian, J., & Yang, R. (2023). Study on a bifunctional switchable metasurface with perfect absorption and polarization conversion based on VO2 and graphene in THz region. Diamond and Related Materials, 110060.

[40] Li, W., Sun, J., Su, C., Gao, P., Wang, X., Liu, X., Xia, F., Zhang, K., Dong, L., & Yun, M. (2023). Dual-pattern broadband polarization converter in THz band based on graphene and VO2 hybrid metasurface. Results in Physics, 107021